International Journal of Heat and Mass Transfer 56 (2013) 525–537

Contents lists available at SciVerse ScienceDirect

International Journal of Heat and Mass Transfer

journal homepage: www.elsevier.com/locate/ijhmt

A kinetic model of droplet heating and evaporation: Effects of inelastic collisions and a non-unity evaporation coefficient

S.S. Sazhin [a,*], J.-F. Xie [a], I.N. Shishkova [b], A.E. Elwardany [a,1], M.R. Heikal [a,2]

[a] Sir Harry Ricardo Laboratories, Centre for Automotive Engineering, School of Computing, Engineering and Mathematics, Faculty of Science and Engineering, University of Brighton, Brighton, BN2 4GJ, UK
[b] Low Temperature Department, Moscow Power Engineering Institute, Krasnokazarmennaya 14, Moscow 111250, Russia

ARTICLE INFO

Article history:
Received 27 July 2012
Received in revised form 19 September 2012
Accepted 21 September 2012

Keywords:
Droplets
Heating
Evaporation
Kinetic modelling
Inelastic collisions
N-dodecane
Evaporation coefficient

ABSTRACT

The previously developed kinetic model for droplet heating and evaporation into a high pressure air is generalised to take into account the combined effects of inelastic collisions between molecules in the kinetic region, a non-unity evaporation coefficient and temperature gradient inside droplets. It is pointed out that for the parameters typical for Diesel engine-like conditions, the heat flux in the kinetic region is a linear function of the vapour temperature at the outer boundary of this region, but practically does not depend on vapour density at this boundary for all models, including and not including the effects of inelastic collisions, and including and not including the effects of a non-unity evaporation coefficient. For any given temperature at the outer boundary of the kinetic region the values of the heat flux are shown to decrease with increasing numbers of internal degrees of freedom of the molecules. The rate of this decrease is strong for small numbers of these degrees of freedom but negligible when the number of these degrees exceeds 20. This allows us to restrict the analysis to the first 20 arbitrarily chosen degrees of freedom of n-dodecane molecules when considering the effects of inelastic collisions. The mass flux at this boundary decreases almost linearly with increasing vapour density at the same location for all above-mentioned models. For any given vapour density at the outer boundary of the kinetic region the values of the mass flux are smaller for the model, taking into account the contribution of internal degrees of freedom, than for the model ignoring these degrees of freedom. It is shown that the effects of inelastic collisions lead to stronger increase in the predicted droplet evaporation time in Diesel engine-like conditions relative to the hydrodynamic model, compared with the similar increase predicted by the kinetic model considering only elastic collisions. The effects of a non-unity evaporation coefficient are shown to be noticeable for gas temperatures of 1500 K. The application of the rigorous kinetic model, taking into account the effects of inelastic collisions and a non-unity evaporation coefficient, and the model taking into account the temperature gradient inside droplets, is recommended when accurate predictions of the values of droplet surface temperature and evaporation time in Diesel engine-like conditions are essential.

1. Introduction

Langmuir [1] was perhaps the first to pay attention to the existence of a 'concentration drop' in the vicinity of the surface of an evaporating solid. This phenomenon was further investigated in a number of papers summarised in [2]. It was pointed out that the gradients of temperature and vapour concentration rise sharply in the immediate vicinity of heated (or cooled) and evaporating surfaces (liquid or solid). The thickness of the layer where this rise takes place was estimated to be of the order of several mean free paths ℓ. Assuming that this thickness is equal to ℓ, the rate of evaporation from the surface was considered to be the same as that into a vacuum. This rate of evaporation was assumed to be equal to the loss of vapour into the surrounding space by diffusion. Surprisingly, this simple model and its minor modifications are still widely used in the modelling of droplet heating and evaporation processes (e.g. [3,4]).

An overview of more recent further developments of this approach to the modelling of droplet heating and evaporation is presented in [5,6]. The most advanced of these developments, based on the direct numerical solution to the Boltzmann equations for fuel vapour and air (background gas) in the vicinity of droplets with the relevant boundary conditions, was described in [7–9]. In these papers, two regions of gas above the surface of the evaporating droplet were considered: the kinetic (in the vicinity of the droplet surface) and hydrodynamic regions. In the most

* Corresponding author. Tel.: +44 (0) 1273642677; fax: +44 (0) 1273642330.
E-mail address: S.Sazhin@brighton.ac.uk (S.S. Sazhin).
[1] Current address: King Abdullah University of Science and Technology, 4700, Thuwal 23955-6900, Saudi Arabia.
[2] Current address: Department of Mechanical Engineering, Universiti of Teknologies, PETRONAS, Bandar Sri Iskandar, 31750 Tronoh, Perak Darul Ridzuan, Malaysia.

0017-9310/$ - see front matter Crown Copyright © 2012 Published by Elsevier Ltd. All rights reserved.
http://dx.doi.org/10.1016/j.ijheatmasstransfer.2012.09.046

Nomenclature

$\mathbf{A}$	transformation matrix in Eq. (27)
a_{ij}	components of $\mathbf{A}$
B_M	Spalding mass transfer number
B_T	Spalding heat transfer number
c	specific heat capacity
C_F	friction drag coefficient
D	diffusion coefficient
E	energy
$\mathbf{E}$	unit matrix
f	molecular distribution function
f_n	parameter introduced in Eq. (6)
h	convection heat transfer coefficient
h_0	parameter defined by Eq. (10)
$\mathbf{j}$	mass flux
J	collisional integral
k	thermal conductivity
k_B	Boltzmann constant
Kn	Knudsen number
ℓ	mean free molecular path
L	latent heat of evaporation
Le	Lewis number
M	molar mass or total number of cells
N	number of degrees of freedom
N_A	Avogadro number
p	pressure or momentum
Pe	Peclet number
Pr	Prandtl number
$\mathbf{q}$	heat flux
q_n	parameter defined by Eq. (11)
r	$\sqrt{\sum_{i=1}^{i=N} E_i}$
$\mathbf{r}$	position
R	distance from the droplet centre
R_d	droplet radius
R_u	universal gas constant
R_v	gas constant referring to vapour
Re	Reynolds number
t	time
T	temperature
$\tilde{T}$	$(T_r - 300)/300$
$\tilde{T}_{Rd}$	T_{Rd}/T_s
U_s	maximal surface velocity
$\mathbf{v}$	velocity vector
v_n	eigenfunctions
x_i	coordinates of vector $\mathbf{X}$
X	molar fraction
$\mathbf{X}$	vector in N-dimensional space
Y	mass fraction

Greek symbols

β	evaporation coefficient
δ_{Rd}	thickness of the kinetic region
Δt	timestep
ΔU	$\lvert U_g - U_d \rvert$
ε	Lennard-Jones parameter
$\mathbf{\Theta}_n$	function defined by Eq. (6)
κ	thermal diffusivity
λ, λ_n	eigenvalues defined by Eq. (9)
μ	dynamic viscosity
$\mu_0(t)$	parameter defined by Eq. (7)
ξ	R/R_d
ρ	density
$\tilde{\rho}_{Rd}$	ρ_{Rd}/ρ_s
σ_{va}	parameter introduced in Eq. (20)
φ	parameter defined by Eq. (24)
Φ	parameter used in the definition of k_{mix}
χ	parameter defined by Eq. (13)
$\Omega_{D,va}$	parameter introduced in Eq. (20)

Subscripts

a	air
amb	ambient
b	boiling
cr	critical
d	droplet
e	evaporation
eff	effective
f	total
g	gas
h	hydrodynamic
i	degrees of freedom
k	kinetic
l	liquid
mix	mixture
out	outgoing
p	constant pressure
r	reference or reflected
Rd	interface between kinetic and hydrodynamic regions
s	surface or swelling
v	vapour
0	initial, reference or at the beginning of a timestep
1	at the end of a timestep

Superscripts

T	transpose
$'$	after collisions
$\sim$	normalised
$-$	average

comprehensive model, described by Sazhin and Shishkova [9], it was assumed that both mass and heat transfer processes in the kinetic region were taken into account.

In our most recent paper [10], simple approximate formulae describing temporal evolution of Diesel fuel droplet radii and temperatures predicted by the kinetic model were suggested. These formulae are valid in the range of gas temperatures relevant to Diesel engine-like conditions and fixed values of initial droplet radii, or in the range of initial droplet radii relevant to Diesel engine-like conditions and fixed values of gas temperature. The new approximations were shown to be reasonably accurate for predicting the temporal evolution of droplet radii and droplet evaporation times. The predictions of droplet temperatures turned out to be less accurate than those of droplet radii, but this accuracy was believed to be sufficient for many practical applications. The application of these formulae is expected to reduce dramatically the CPU requirements of kinetic modelling, which can potentially open the way to the implementation of the kinetic models into engineering computational fluid dynamics (CFD) codes designed to model droplet heating and evaporation in a realistic engineering environment, including that of Diesel engines (e.g. see [11,12]).

Although considerable progress in the development of kinetic models of droplet heating and evaporation was reported in [7–10], all these models were based on a number of restrictive assumptions. Firstly, in all these models it was assumed that there is no temperature gradient inside droplets. The limitations of this assumption have been widely discussed in the literature, using the conventional hydrodynamic approach (e.g. [13–15]). Nobody,

however, to the best of our knowledge, has considered this effect in conjunction with kinetic modelling. Secondly, the kinetic models, described in [7–10], were based on the assumption that all collisions between molecules are elastic. This assumption could be justified in the case of monoatomic molecules such as Argon, but in the case of complex molecules, such as n-dodecane $C_{12}H_{26}$ (the nearest approximation to Diesel fuel), this assumption becomes highly doubtful. A new approach to the solution of the Boltzmann equation in the presence of inelastic collisions was suggested in [16], but this approach has not yet been applied to the modelling of heating and evaporation of droplets. Thirdly, in the models described in [7–10] it was assumed that the evaporation coefficient is equal to 1, which could not be rigorously justified. Moreover, in our recent papers it was shown that this coefficient can be well below 1 (close to 0.5) especially when temperatures are close to critical [17–19].

The aim of this paper is to develop further the kinetic model described in [5–10] in which these assumptions are relaxed. We will restrict our analysis to stationary droplets and ignore the effects of the moving boundary due to evaporation (see [20–22] for the analysis of this effect), the formation of the thermal boundary layer around droplets (see [23] for details) and the effects of thermal radiation [6].

In Section 2 the physical models used in various regions inside and around droplets are described. The model used for the analysis of the effects of inelastic collisions is presented and discussed in Section 3, following [16]. The algorithm used for calculations is briefly described in Section 4. The values of droplet temperatures and radii predicted by various models, but assuming that the evaporation coefficient is equal to 1, are compared in Section 5. The modifications of these results in the case when the evaporation coefficient is not equal to 1 are presented and discussed in Section 6. The main results of the paper are summarised in Section 7.

2. Physical models

As in [7–10], two regions of gas above the surface of the evaporating fuel droplet are considered: the kinetic and hydrodynamic regions. In contrast to [7–10], we relax the assumption that the liquid thermal conductivity is infinitely large and consider the processes in the liquid phase region as well. All three regions are schematically shown in Fig. 1. As in [7–10], we assume that gas consists of two components, fuel vapour and background air, both in the kinetic and hydrodynamic regions. It is assumed that the contribution of chemical reactions of fuel vapour and oxygen can be ignored. Fuel vapour and air dynamics in the kinetic region are described by the Boltzmann equations, while the conventional hydrodynamic analysis is applied in the hydrodynamic region.

As in [7–10], the effects of the curvature of the droplet surface are ignored in the analysis. This is justified by the fact that the thickness of the kinetic region is very small, not more than 10–100 ℓ. Note that although in this case the conventional Knudsen number $Kn = \ell/R_d$, where R_d is the droplet radius, becomes infinitely small, the kinetic effects cannot be *a priori* ignored. This phenomenon has been discussed by a number of authors (e.g. [24–29]) and is confirmed by the results of our analysis.

The models used in all three regions and the conditions at the interface between the regions are discussed in the following three sections.

2.1. Liquid phase region

The models for droplet heating used in [14,15] were implicitly based on the assumptions that the evaporation rate of droplets is small and the value of droplet radius R_d does not change during any time step (although this radius changes from one step to another). This means that the effect of a moving boundary on droplet heating was ignored. This is a well known approach used in all available CFD codes (e.g. [30]). Two approaches were developed to take into account the changes in droplet radius R_d during the time steps. Firstly it was assumed that R_d is a linear function of time. Secondly, the evolution of droplet temperature was calculated for an *a priori* fixed function $R_d(t)$ [20,21]. These effects, however, will not be taken into account in the present analysis.

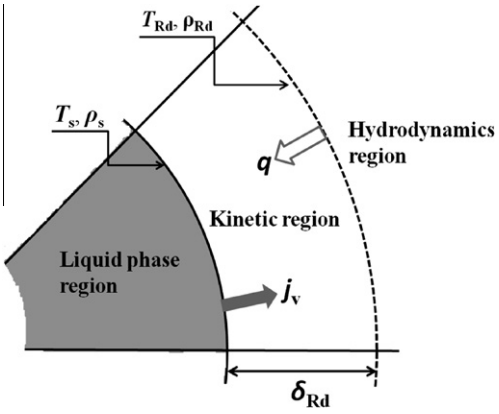

Fig. 1. Liquid phase, kinetic and hydrodynamic regions in the vicinity of the surface of the droplet. T_s is the droplet surface temperature, ρ_s is the vapour density in the immediate vicinity of the droplet surface, T_{Rd} and ρ_{Rd} are the temperature and density of vapour at the outer boundary of the kinetic region. δ_{Rd} indicates the thickness of the kinetic region, $\mathbf{j_v}$ and $\mathbf{q}$ show the directions of the vapour mass and heat fluxes, respectively.

Assuming that the droplet heating process is spherically symmetric, the droplet temperature ($T \equiv T(t,R)$) can be found from the solution to the equation for T in the form [31,32]:

$$\frac{\partial T}{\partial t} = \kappa\left(\frac{\partial^2 T}{\partial R^2} + \frac{2}{R}\frac{\partial T}{\partial R}\right) \tag{1}$$

for $0 \leqslant t < t_e$, $0 \leqslant R < R_d(t)$, where κ is the liquid thermal diffusivity ($\kappa = k_l/(c_l\rho_l)$), k_l is the thermal conductivity, c_l is the specific heat capacity, ρ_l is the density, R is the distance from the centre of the droplet, t_e is the evaporation time. The effect of thermal radiation is ignored.

Remembering the physical background to the problem, we look for the solution to this equation in the form of a twice continuously differentiable function $T \equiv T(t,R)$ for $0 \leqslant t < t_e$, $0 \leqslant R < R_d(t)$. This solution should satisfy the boundary condition:

$$\left(k_l\frac{\partial T}{\partial R} + hT\right)\Big|_{R=R_d(t)} = hT_g + \rho_l L\dot{R}_{de}(t), \tag{2}$$

T is finite and continuous at $R \to 0$, $T_s = T(R_d(t),t)$ is the droplet's surface temperature, L is the latent heat of evaporation, h is the convection heat transfer coefficient, $\dot{R}_{de}(t) \leqslant 0$ is the rate of change of droplet radius due to evaporation. Eq. (2) is the energy balance condition at $R = R_d(t)$. The initial condition is taken in the form:

$$T(t=0) = T_0(R), \tag{3}$$

where $0 \leqslant R \leqslant R_{d0} = R_d(t=0)$. In conventional hydrodynamic models, the value of $R_d(t)$ is controlled by vapour diffusion from the droplet surface and droplet thermal swelling. In our model, it is controlled by vapour diffusion from the interface between the kinetic and hydrodynamic regions (see Fig. 1) and swelling, and can be found from the equation [6]:

$$\dot{R}_d \equiv \dot{R}_{de} + \dot{R}_{ds} = -\frac{D_g\rho_{\text{total}}\ln(1+B_M)}{\rho_l R_d} + \frac{R_{d0}}{\Delta t}\left[\left(\frac{\rho(\overline{T}_0)}{\rho(\overline{T}_1)}\right)^{1/3} - 1\right], \tag{4}$$

where $\dot{R}_{ds}$ is the rate of change of droplet radius due to swelling (or contraction), $B_M = Y_{vRd}/(1 - Y_{vRd})$ is the Spalding mass transfer number (assuming that there is no vapour in the ambient gas), Y_{vRd} is the mass fraction of vapour at the interface between the kinetic and hydrodynamic regions, which is ultimately controlled by gas temperature in this region (T_{Rd}) [6], $\overline{T}_0$ and $\overline{T}_1$ are average droplet temperatures at the beginning and the end of the time step Δt, ρ are the corresponding densities.

The first term on the right hand side of Eq. (4) follows from a well known expression for the mass evaporation rate $\dot{m}_d$ (see Eq. (7) of [6]): $\dot{R}_{de} = \dot{m}_d/\left(4\pi R_d^2 \rho_l\right)$. The second term is found from the relation:

$$\dot{R}_{ds} = \frac{R_{d1} - R_{d0}}{\Delta t} = \frac{R_{d0}}{\Delta t}\left(\frac{R_{d1}}{R_{d0}} - 1\right) = \frac{R_{d0}}{\Delta t}\left[\left(\frac{\rho(\overline{T}_0)}{\rho(\overline{T}_1)}\right)^{1/3} - 1\right].$$

At the last step of the derivation of this formula it was taken into account that the total mass of the droplet is conserved during swelling.

When deriving (4) we ignored the difference between R_d and $R_d + \delta_{Rd}$. The validity of this assumption was checked by a direct comparison of the results, taking and not taking into account the effects of the sphericity of droplets for thickness of the kinetic region equal to ten mean molecular paths, calculated for pressure equal to 30 bars (Diesel engine-like conditions) and temperatures equal to fuel droplet surface temperatures (see Section 3.1 and Eq. (11) of [8]).

Assuming that R_d is fixed during the time step, the analytical solution to Eq. (1) subject to the above boundary and initial conditions was obtained in the form [33]

$$T(R) = \frac{1}{R\sqrt{R_d}}\left[\sum_{n=1}^{\infty}\Theta_n(t)\sin\left(\lambda_n\frac{R}{R_d}\right) + \frac{\mu_0(t)}{1+h_0}\frac{R}{R_d}\right], \tag{5}$$

where

$$\Theta_n(t) = \Theta_n(0)\exp\left[-\frac{\kappa\lambda_n^2 t}{R_{d0}^2}\right] + f_n\int_0^t \frac{\mathrm{d}\mu_0(\tau)}{\mathrm{d}\tau}\exp\left[-\frac{\kappa\lambda_n^2(t-\tau)}{R_{d0}^2}\right]\mathrm{d}\tau, \tag{6}$$

$$\mu_0(t) \equiv R_d^{5/2}\frac{h}{k_l}T_g, \tag{7}$$

$$f_n = -\frac{\sin\lambda_n}{\|\nu_n\|^2\lambda_n^2}, \nu_n(\xi) = \sin\lambda_n\xi \quad (n = 1,2,\ldots).$$

$$\|\nu_n\|^2 = \frac{1}{2}\left(1 - \frac{\sin 2\lambda_n}{2\lambda_n}\right) = \frac{1}{2}\left(1 + \frac{h_0}{h_0^2 + \lambda_n^2}\right). \tag{8}$$

$\xi = R/R_d$, λ_n are positive solutions to the equation

$$\lambda\cos\lambda + h_0\sin\lambda = 0 \tag{9}$$

presented in ascending order,

$$h_0 = \frac{h}{k_l}R_d - 1 \tag{10}$$

is assumed to be constant during the time step,

$$\Theta_n(0) = q_n + \mu_0(0)f_n,$$
$$q_n = \frac{1}{\|\nu_n\|^2}\int_0^1 R_{d0}^{3/2}\xi T_0(\xi R_{d0})\nu_n(\xi)\mathrm{d}\xi. \tag{11}$$

The effect of recirculation inside droplets was taken into account based on the effective thermal conductivity (ETC) model [34] in which the liquid thermal conductivity k_l is replaced by the effective thermal conductivity

$$k_{\mathrm{eff}} = \chi k_l, \tag{12}$$

where the coefficient χ is defined as

$$\chi = 1.86 + 0.86\tanh[2.245\log_{10}(\mathrm{Pe}_{d(l)}/30)], \tag{13}$$

$\mathrm{Pe}_{d(l)} = \mathrm{Re}_{d(l)}\mathrm{Pr}_l$ is the droplet Peclet number, in which liquid transport properties and the maximum surface velocity inside droplets were used. The latter velocity was calculated as [34]:

$$U_s = \frac{1}{32}\Delta U\left(\frac{\mu_g}{\mu_l}\right)\mathrm{Re}_d C_F, \tag{14}$$

where $\Delta U \equiv |U_g - U_d|$ is the relative velocity between ambient gas and droplets, $\mu_{g(l)}$ is the dynamic viscosity of gas (liquid), Re_d is the droplet Reynolds number based on the droplet diameter, C_F is the friction drag coefficient estimated as [34]:

$$C_F = \frac{12.69}{\mathrm{Re}_d^{2/3}(1 + B_M)}. \tag{15}$$

It can be shown that in the limit $k_l \to \infty$, Solution (5) reduces to [35]:

$$T_d = T_g + (T_{d0} - T_g)\exp\left(-\frac{3ht}{c_l\rho_l R_d}\right), \tag{16}$$

where T_d does not depend on R.

Eq. (16) was used in the previously reported kinetic models of droplet heating and evaporation [7–10]. The model presented in this paper will be based on Eq. (5). The results presented by the models based on both equations will be compared where appropriate.

The following approximations for n-dodecane are used, following [36]:

$$L = 37440\cdot(T_{\mathrm{cr}} - T_s)^{0.38}\ \mathrm{J/kg},$$
$$\rho_l = 744.11 - 0.771\cdot(T - 300)\quad \mathrm{kg/m^3},$$
$$c_l = 2180 + 4.1\cdot(T - 300)\quad \mathrm{J/(kg\cdot K)},$$

where $T_{\mathrm{cr}} = 659$ K is the n-dodecane critical temperature.

These and other properties used in the paper were compiled from different sources, including [37,38].

When calculating average liquid density and specific heat capacity, T in the last two expressions is replaced with the average temperature $\overline{T}$.

2.2. Kinetic region

As in [7–10], the evolution of the molecular velocity distribution functions of air $f_a \equiv f_a(\mathbf{r}, t, \mathbf{v})$ and vapour $f_v \equiv f_v(\mathbf{r}, t, \mathbf{v})$ in the kinetic region is controlled by the corresponding Boltzmann equations:

$$\left.\begin{aligned}\frac{\partial f_a}{\partial t} + \mathbf{v}_a\frac{\partial f_a}{\partial \mathbf{r}} = J_{aa} + J_{av}\\ \frac{\partial f_v}{\partial t} + \mathbf{v}_v\frac{\partial f_v}{\partial \mathbf{r}} = J_{va} + J_{vv}\end{aligned}\right\}, \tag{17}$$

where $J_{\alpha\beta}$ ($\alpha = a, v$; $\beta = a, v$) are collision integrals, taking into account the contribution of the collisions between molecules. Our approach to the solution of these equations, taking into account the effects of inelastic collisions, is discussed in Section 3.

Eqs. (17) are solved subject to the boundary conditions at the interface between the kinetic and liquid phase regions and at the interface between the kinetic and hydrodynamic regions. The first boundary condition for the fuel vapour can be presented as:

$$f_{v\,(\mathrm{out})} = \beta f_{vs} + (1 - \beta)f_{vr}, \tag{18}$$

where f_{vs} is the distribution function of molecules leaving the liquid surface assuming that $\beta = 1$, f_{vr} is the distribution function of reflected molecules. Both f_{vs} and f_{vr} are assumed to be isotropic Maxwellian. The temperature for f_{vs} is assumed to be equal to T_s, while the temperature for f_{vr} is assumed to be equal to T_{Rd}. This is jus-

tified by the fact that the thickness of the kinetic region is small and the gas temperature just above the droplet surface is close to T_{Rd}[2].

As shown in [19], a more accurate approximation for f_{vr} would have been a bi-Maxwellian distribution, but this effect is not taken into account in our paper.

At the boundary between the kinetic and hydrodynamic regions the distribution function of both fuel vapour and air molecules entering the kinetic region is assumed to be Maxwellian, controlled by ρ_{Rd} and T_{Rd}. Further details of the boundary conditions used for kinetic calculations are discussed in [8].

The contributions of both mass and heat transfer in the kinetic region are taken into account following the approach described in [9]. At first, as in [7–10], it will be assumed that the evaporation coefficient β is equal to 1. Then the effects of realistic β on droplet heating and evaporation will be investigated.

2.3. Hydrodynamic region

As in [7–10], it is assumed that the mass fluxes leaving the kinetic region and the corresponding diffusion fluxes in the hydrodynamic region are matched.

$$\frac{M_v}{N_A}\int_{-\infty}^{+\infty} dv_y \int_{-\infty}^{+\infty} dv_z \int_{0}^{+\infty} dv_x v_x f_v(\mathbf{r},t,\mathbf{v}) = \frac{\rho_{\text{total}} D_{va}}{R_d}\ln(1+B_M) \equiv j_h = j_v, \tag{19}$$

where ρ_{total} is the density of the mixture of air and vapour at the inner boundary of the hydrodynamic region ($\rho_{\text{total}} = \rho_{vRd}/Y_{vRd}$), D_{va} is the binary diffusion coefficient (diffusion of vapour through air), j_h is the mass flux of evaporated fuel. B_M takes into account the effect of the finite mass fraction of fuel vapour on the evaporation process. The binary diffusion coefficient is calculated from the following expression [39]:

$$D_{va} = 1.8583\times 10^{-7}\sqrt{T_r^3\left(\frac{1}{M_v}+\frac{1}{M_a}\right)}\frac{1}{p\,\sigma_{va}^2\Omega_{D,va}}, \tag{20}$$

where D_{va} is in m^2/s, p is in atm (1 atm $\approx 1.01\times 10^5$ Pa), $\sigma_{va} = 0.5(\sigma_v + \sigma_a)$ is the average diameter of molecules of vapour and air (in $m\times 10^{-10}$), $\Omega_{D,va}$ is the function of $T^* \equiv k_B T_r/\varepsilon_{va}$, $\varepsilon_{va} = \sqrt{\varepsilon_v \varepsilon_a}$, ε_v and ε_a are Lennard-Jones parameters for fuel vapour and air [34], k_B is the Boltzmann constant, $T_r = T_s + \frac{1}{3}(T_g - T_s)$ is the reference temperature, T_s is the droplet surface temperature, T_g is the ambient gas temperature.

In accordance with [39] the following approximation for $\Omega_{D,va}$ is used:

$$\Omega_{D,va} = \frac{1.06036}{T^{*0.15610}} + \frac{0.19300}{\exp(0.47635T^*)} + \frac{1.03587}{\exp(1.52996T^*)} + \frac{1.76474}{\exp(3.89411T^*)}.$$

As in [9], the following values are used for most of our analysis: $\sigma_v = 9.373\times 10^{-10}$m, $\sigma_a = 3.667\times 10^{-10}$m, $\varepsilon_v/k_B = 351.0$ K, and $\varepsilon_a/k_B = 97.0$ K [34].

The heat flux supplied to the droplet is estimated as:

$$q_s = h(T_g - T_{Rd}), \tag{21}$$

where, as in [9], the convection heat transfer coefficient h is obtained from the equation:

$$h = \frac{k_{\text{mix}}}{R_d}\frac{\ln(1+B_T)}{B_T}, \tag{22}$$

k_{mix} is the thermal conductivity of the mixture of vapour and air, B_T is the Spalding heat transfer number calculated as [6]:

$$B_T = (1+B_M)^{\varphi} - 1, \tag{23}$$

$$\varphi = \left(\frac{c_{pv}}{c_{pg}}\right)\frac{1}{\text{Le}} = \frac{c_{pv}\rho_{\text{mix}}D_{va}}{k_{\text{mix}}}. \tag{24}$$

$\text{Le} = k_{\text{mix}}/(c_{pg}\rho_{\text{mix}}D_{va})$ is the Lewis number, c_{pv} and c_{pg} are specific heat capacities of the fuel vapour and ambient gas (air), respectively. Note that φ does not depend on c_{pg}. Eq. (24) is strictly speaking valid for stationary droplets only [34]. However, as shown in [40] the values of average droplet temperatures calculated using this formula are almost indistinguishable from the values predicted by the models, taking into account the non-zero droplet velocities.

Based on [9] the following approximations for c_{pv}, k_v and k_a are used

$$c_{pv} = 1594.60 + 1.15\tilde{T} - 100.56\tilde{T}^2 - 28.56\tilde{T}^3 + 5.07\tilde{T}^4 - 0.25\tilde{T}^5 \text{ J/(kg·K)},$$
$$k_v = 0.02667\cdot(T_r/300) - 0.02087 \text{ W/(m K)},$$
$$k_a = 3.227\cdot 10^{-3} + 8.3894\cdot 10^{-5}\cdot T_r - 1.9858\cdot 10^{-8}\cdot T_r^2 \text{ W/(mK)},$$

where $\tilde{T} = (T_r - 300)/300$, T_r is the reference temperature, defined earlier.

The thermal conductivity of the mixture of fuel vapour and air is estimated as [9]

$$k_{\text{mix}} = \sum_{i=1}^{2}\frac{X_i k_i}{\sum_{j=1}^{2} X_j \Phi_{ij}} \text{ W/(m K)},$$

where i and j stand for fuel vapour or air, X_i and X_j are molar fractions of species i and j,

$$\Phi_{ij} = \frac{1}{\sqrt{8}}\left(1+\frac{M_i}{M_j}\right)^{-1/2}\left[1+\left(\frac{k_i}{k_j}\right)^{1/2}\left(\frac{M_j}{M_i}\right)^{1/4}\right]^2,$$

$M_{i,j}$ are molar masses of the corresponding species ($M_v = 170.3$ kg/kmol, $M_a = 28.97$ kg/kmol [34]).

Following [9], the values of the saturated fuel vapour pressure are estimated as:

$$p_{v\,(\text{sat})} = A_1\cdot\exp\left(\frac{T_s - A_0}{B_1}\right) \text{ Pa}, \tag{25}$$

where

$$\left.\begin{aligned} A_0 &= 300.17542\\ A_1 &= 70.44441\\ B_1 &= 22.36885 \end{aligned}\right\} \text{ when } T_s \le 440 \text{ K}$$

$$\left.\begin{aligned} A_0 &= 449.87125\\ A_1 &= 46204.48272\\ B_1 &= 56.97142 \end{aligned}\right\} \text{ when } T_s > 440 \text{ K}.$$

Eq. (25) is an alternative presentation of the Clausius–Clapeyron equation [41]. Note that there is a typo in the corresponding equation presented in [9].

The processes in the kinetic and hydrodynamic regions are linked by the matching conditions of conservation of mass flux (see Eq. (19)) and heat flux

$$q_k = q_h, \tag{26}$$

at the interface. Subscripts $_k$ and $_h$ refer to kinetic and hydrodynamic regions respectively.

Note that Figs. 7–13 of [9] were based on a simplified version of the above model for the hydrodynamic region. Namely, it was assumed that $\Omega_{D,va} = T^*$, $\varphi = 1$, $L = 250000$ J/kg, $\rho_l = 586$ kg/m^3, $c_l = 2900$ J/(kg K), and $k_{\text{mix}} = 0.035$ J/(m K). These simplifications were justified by the fact that the main focus of [9] was on the comparison of the predictions of hydrodynamic and kinetic models

rather than on the most accurate predictions of droplet radii and temperature during the heating and evaporation processes. In the current paper, a considerably improved model is used as described above.

3. Effects of inelastic collisions

In our previous papers [7–10], it was assumed that molecules can be approximated as hard elastic spheres. In contrast to these papers, however, we take into account the inelastic effects during the collisions of these spheres, using a well known inelastic hard spheres (IHS) model (see [42]). The details of our model for inelastic collisions are given in [16]. Here the focus will be on a brief summary of the background to the problem and this model.

Probably the first phenomenological model for binary collisions in a gas mixture having continuous internal energy was developed by Borgnakke and Larsen [43]. This model was applied to the Monte Carlo simulation of rarefied gas flows. Since the publication of this paper, a substantial number of papers have been published, in which various models of inelastic collision have been considered. These are some examples: [44–54].

The model used in this paper is different from those suggested earlier, although it is based on some widely used assumptions, such as the approximation of molecules by inelastic hard spheres (IHS). Although this model has been tested for some rather specific problems, its nature is rather general and it can be applied to any molecules with arbitrary large numbers of internal degrees of freedom. This model, however, is expected to be the most effective for the analysis of such complex molecules as n-dodecane, considered in our previous papers.

Let us consider two colliding molecules. Regardless of the nature of the collision between them, their centre of mass is not affected by this collision. The state of the molecules after the collision is described in the reference system linked with this centre of mass. In this system, each of these molecules has three translational and a certain number of internal degrees of freedom, so that the total number of degrees of freedom of both molecules is equal to N. During the collisions, the energy of each molecule is redistributed between the degrees of freedom, but the total number of degrees of freedom remains the same. Let us assume that none of these degrees of freedom is preferable to any of the others. This allows us to consider the redistribution of energy between these degrees of freedom during the collision process as random. For each of these degrees of freedom we allocate one dimension in the $N-$dimensional space describing all degrees of freedom. Once we have done this, we consider a sphere in this space with its centre at the origin (where energies of all degrees of freedom are equal to zero) and radius given by the following expression: $r=\sqrt{\sum_{i=1}^{i=N}E_i}$, where E_i is the energy of the ith degree of freedom (translational or internal). Since r^2 gives the total energy of the system E_f, this equation can be considered as an equation of the conservation of energy at the surface of the sphere in the centre of mass system of reference.

The location of the points on the surface of this sphere can be described by an $N-$dimensional vector $\mathbf{X}=(x_1,x_2,\ldots x_N)$ with the basis $(\mathbf{e}_1,\mathbf{e}_2,\ldots\mathbf{e}_N)$ and the norm $\|\mathbf{X}\|=r=\sqrt{E_f}$. The redistribution of energy between the degrees of freedom during the collision process can be described in terms of the rotation of vector $\mathbf{X}$ in the N-dimensional space. If none of the degrees of freedom is preferable to any of the others, then this rotation of the vector $\mathbf{X}$ can be considered as random. In the most general form it can be described by the following equation:

$$\mathbf{X}'=\mathbf{A}\mathbf{X}, \tag{27}$$

where $\mathbf{X}'$ is the new position of vector $\mathbf{X}$ after rotation, $\mathbf{A}$ is the rotation matrix:

$$\mathbf{A}=\begin{bmatrix} a_{11} & a_{12} & \ldots & a_{1N} \\ a_{21} & a_{22} & \ldots & a_{2N} \\ \ldots & \ldots & \ldots & \ldots \\ a_{N1} & a_{N2} & \ldots & a_{NN} \end{bmatrix}.$$

The conservation of the total energy during the collision process implies that vector $\mathbf{X}'$ remains at the surface of the sphere of radius r. This is possible if and only if

$$\mathbf{A}^{\mathbf{T}}\mathbf{A}=\mathbf{E}, \tag{28}$$

where $\mathbf{A}^{\mathbf{T}}$ is the transpose of the matrix $\mathbf{A}$, $\mathbf{E}$ is the unit matrix.

Eq. (28) can be presented in a more explicit form as the combination of the following systems of equations

$$\left.\begin{aligned} &a_{11}^2+a_{21}^2+\ldots+a_{N1}^2=1\\ &a_{12}^2+a_{22}^2+\ldots+a_{N2}^2=1\\ &\ldots\\ &a_{1N}^2+a_{2N}^2+\ldots+a_{NN}^2=1 \end{aligned}\right\}, \tag{29}$$

$$\left.\begin{aligned} &a_{11}a_{12}+a_{21}a_{22}+\ldots+a_{N1}a_{N2}=0\\ &a_{11}a_{13}+a_{21}a_{23}+\ldots+a_{N1}a_{N3}=0\\ &\ldots\\ &a_{11}a_{1N}+a_{21}a_{2N}+\ldots+a_{N1}a_{NN}=0 \end{aligned}\right\}, \tag{30}$$

$$\ldots$$

$$a_{1(N-1)}a_{1N}+a_{2(N-1)}a_{2N}+\ldots.+a_{N(N-1)}a_{NN}=0. \tag{31}$$

When writing Eqs. (30) and (31) identical equations have been excluded. The total number of Eqs. (30) and (31) is

$$(N-1)+(N-2)+(N-3)+\ldots.+1=\frac{N}{2}(N-1)$$

for N^2 unknown coefficients a_{ij}. This allows us to take randomly $N^2-\frac{N}{2}(N-1)=\frac{N}{2}(N+1)$ of these coefficients with an additional restriction imposed by Eq. (29) (normalisation condition).

The following procedure for the construction of the components matrix $\mathbf{A}$ is suggested.

1. The coefficients $a_{11}, a_{21}, \ldots, a_{N1}$ are arbitrarily chosen but normalised based on the first equation in System (29).
2. The coefficients $a_{12}, a_{22}, \ldots, a_{(N-1)2}$ are arbitrarily chosen, while the value of the coefficient a_{N2} is found from the first equation of System (30):

$$a_{N2}=-\frac{1}{a_{N1}}(a_{11}a_{12}+a_{21}a_{22}+\cdots+a_{(N-1)1}a_{(N-1)2}). \tag{32}$$

Then all coefficients are normalised based on the second equation in System (29).

Following the same procedure all other components of the matrix $\mathbf{A}$ are found, and this allows us to calculate $\mathbf{X}'$ based on Eq. (29).

The numerical algorithm used in the analysis is based on the method of direct numerical solution of the Boltzmann equation, described in [55,56]. It includes the following steps. Physical and velocity spaces are discretised along with time. Time and physical space are discretised as in conventional structured computational fluid dynamics (CFD) codes. The discretisation of the velocity space is performed similarly to the physical space by replacing continuous values of $\mathbf{v}$ with a discrete set $\{\mathbf{v}^k\}^M$, where k indicates the position of a velocity cell, M is the total number of cells. The boundaries of the velocity domain in v_x, v_y, v_z directions are chosen in such a way that the contribution of molecules with velocities

outside this range can be ignored. The difference between minimal and maximal values of the velocities was taken to be equal to 5 or 6 average thermal speeds $\sqrt{2R_\alpha T_\alpha}$. Due to the difference in R_α for different gas components, the ranges of velocities for these components are also different.

For each value of $\mathbf{v}_\alpha^k$, the corresponding value of f_α^k is specified. This allows us to present Eq. (17) for each gas component in a discretised form:

$$\left\{\begin{array}{l} \frac{\Delta f_\alpha^1}{\Delta t}+\mathbf{v}_\alpha^1\frac{\Delta f_\alpha^1}{\Delta \mathbf{r}}=J_{\alpha\alpha}^1+J_{\alpha\beta}^1 \\ \cdots \\ \frac{\Delta f_\alpha^k}{\Delta t}+\mathbf{v}_\alpha^k\frac{\Delta f_\alpha^k}{\Delta \mathbf{r}}=J_{\alpha\alpha}^k+J_{\alpha\beta}^k \\ \cdots \\ \frac{\Delta f_\alpha^M}{\Delta t}+\mathbf{v}_\alpha^M\frac{\Delta f_\alpha^M}{\Delta \mathbf{r}}=J_{\alpha\alpha}^M+J_{\alpha\beta}^M \end{array}\right\}^M. \tag{33}$$

The boundary and initial conditions for the distribution functions are taken into account.

After calculation of $J_{\alpha\beta}^k$ for each cell $\mathbf{v}_\alpha^k$, the non-linear system of integral–differential equation (17) reduces to the linear system of algebraic Eq. (33), presented for both gas components. Following [55], the numerical solution of System (33) is performed in two steps. Firstly, molecular displacements are calculated ignoring the effect of collisions $\left(J_{\alpha\alpha}^k=J_{\alpha\beta}^k=0\right)$. Secondly, the collisional relaxation is calculated under the assumption of spatial homogeneity.

The numerical solution of Eq. (33) at the first step is performed following the explicit approach. The validity of the Courant condition:

$$\Delta t \max(|v_x|,|v_y|,|v_z|)<\min(\Delta x,\Delta y,\Delta z) \tag{34}$$

is assumed. Condition (34) guarantees that even the fastest molecules cannot cross more than one cell boundary in any of the directions x, y or z.

At the next step, the displacement of molecules stops and they start colliding. Again using the explicit approach, each equation in System (33) can be written as:

$$\frac{f_\alpha^{k,n}-\tilde{f}_\alpha^{k,n-1}}{\Delta t}=J_{\alpha\alpha}^{k,n-1}+J_{\alpha\beta}^{k,n-1}, \tag{35}$$

where $\tilde{}$ indicates the value of the distribution function calculated at the first step, additional superscripts $^{n-1}$ and ^{n} indicate consecutive time steps. Eq. (35) are to be solved in each cell in the physical space.

Further details of the implementation of this algorithm are described in [7].

A model for inelastic collisions, described earlier, allows us to obtain the energies of all degrees of freedom after individual collisions. However, we are interested only in the net change of the kinetic energy of each of two molecules during collisions in the centre of mass reference system. This change in the kinetic energy can be described in terms of the change of the radius of the three dimensional sphere, which is the projection of the N-dimensional sphere on the three-dimensional space, describing the kinetic energies of both colliding molecules in three directions. This is schematically illustrated in Fig. 2 for the case of the projection of the N-dimensional sphere on the two-dimensional plane. Following [7], this space is presented in terms of the components of momenta p_x and p_y of both colliding molecules. Points p and p_* show the positions of molecules before the collision. If the collisions were elastic, then the values of momenta after collisions would lie on the dashed circle shown in Fig. 2, being separated by 180°. Possible values of these momenta after the collisions are shown as empty circles.

As mentioned in [7], randomly chosen directions of molecular momenta after collision are likely to be the values of these momenta lying between the values in the nodes of the discretised momenta space. This eventually can lead to non-conservation of momenta and energies during the collision process. To overcome this problem, following [7] the momenta are discretised not only during the description of molecular motion but also in the analysis of the collision process. Namely, we assume that the momenta after the collisions belong to an *a priori* chosen set of momenta, which are nodes in the momenta space shown in Fig. 2. In the case shown in Fig. 2, in the absence of inelastic collisions, there are 4 such points corresponding to 4 combinations of momenta of molecules after collision. The maximal number of these combinations for the plane is 8. In the three dimensional case, the circumferences shown in Fig. 2 turn into the surfaces of spheres and the maximal number of possible intersection points increases to 24. This corresponds to the maximal total number of combinations of momenta after collision. This approach provides the consistency in discretisation processes used for the description of molecular dynamics and collisions. It has been tested on numerous problems, some of which are discussed in [7–10].

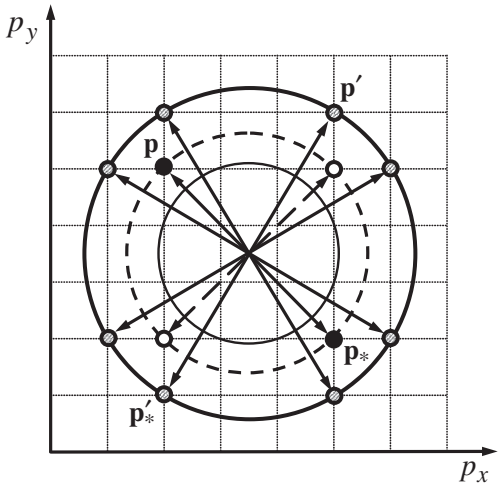

Fig. 2. A projection of the surface of an N-dimensional sphere, describing the energies referring to translational and internal degrees of freedom of two colliding molecules, in a two dimensional space referring to two translational degrees of freedom. $\mathbf{p}$ and $\mathbf{p}^*$ show the locations of the molecular momenta before the collision. The dashed circle shows possible locations of molecular momenta after the collision if the contribution of internal degrees of freedom is ignored. The thin solid circle shows possible locations of molecular momenta after the collision if molecular internal energy increases during the collision. The thick solid circle shows possible locations of molecular momenta after the collision if molecular internal energy decreases during the collision. $\mathbf{p}'$ and $\mathbf{p}^{*\prime}$ show the allowed locations of the molecular momenta after the collision if molecular internal energy decreases during the collision.

If during the collision the net internal energy of molecules increases, this has to be compensated for by a reduction in the kinetic energies of molecules, as the total energy of molecules during the collision is conserved. This leads to the reduction of the radius of the corresponding circle in Fig. 2. In the opposite case, when the net internal energy of molecules decreases, this has to be compensated for by an increase in the kinetic energies of molecules, and also of the radius of the corresponding circle in Fig. 2. Both cases are shown in Fig. 2 by solid circles. In the case of increased net kinetic energy of molecules, possible values of the momenta of both molecules after the collision are shown as the filled black circles. These include points p' and p'_*. The changes of radii of the circles after collision have been calculated based on Korobov's sequences ([57]), enhanced by the randomization of individual points. As in the case of elastic collisions, the points p' and p'_* are chosen to coincide with the nodes of the discretised momenta space.

The model described above could be generalised to the case when the probabilities of excitation of various degrees of freedom are not equal (for example, the three rotational modes are expected to be much more important than the vibrational modes). This could be achieved by introduction of the weighting function, and/or limiting the range of degrees of freedom to be activated. We cannot, however, specify this weighting function in the case of such complex molecules as n-dodecane, for which our model has been primarily developed.

This approach does not include the analysis of specific internal degrees of freedom and can be potentially applicable to any type of inelastic collision. Moreover, the dependence of the effect of inelastic collisions on the number of degrees of freedom was shown for several examples to be strong for a small number of internal degrees of freedom, but rather weak for large numbers of degrees of freedom (more than about 20). This allows us to restrict our analysis to about 20 degrees of freedom when analysing the collisions between complex n-dodecane molecules regardless of the actual number of degrees of freedom. This will be considered in more detail in the next section.

The model described above was validated against the observed distribution of the number density of Nitrogen in the vicinity of a shock wave (see [16] for the details).

4. Solution algorithm

The idea of the solution algorithm used in the analysis is similar to the one described in [9]. As in [9], the first step in the solution of Eq. (17) is to perform an investigation of mass and heat transfer processes in the kinetic region for a set of values of ρ_{Rd} and T_{Rd}. Remembering that we consider the problem of heating and evaporation of droplets in a hot gas, these parameters are assumed to be in the ranges: $\rho_{Rd} < \rho_s$ and $T_{Rd} > T_s$. During the droplet heating process the temperature increases away from the droplet; the evaporation process is possible when the fuel vapour density decreases away from the droplet surface. Once the values of ρ_{Rd} and T_{Rd} have been found, the solution of the Boltzmann equations (17) in the kinetic region allows us to calculate the normalised mass and heat fluxes at the outer boundary of this region:

$$\tilde{j}_k = j_k/(\rho_0\sqrt{R_v T_0}), \quad \tilde{q}_k = q_k/(p_0\sqrt{R_v T_0}),$$

where R_v is the gas constant referring to fuel vapour, T_0 is the reference temperature chosen equal to 600 K, p_0 and ρ_0 are the saturated fuel vapour pressure and density corresponding to T_0, ρ_0 is calculated from the ideal gas law, subscript $_k$ stands for kinetic.

We assume that $\rho_{Rd} = 0.9\rho_s$ and $T_s = T_0 = 600$ K. The values of $\tilde{q}_k$ were calculated for the numbers of internal degrees of freedom N_{int} from 0 to 50 and $\tilde{T}_{Rd} = T_{Rd}/T_s$ from 1 to 1.4. The results are shown in Fig. 3. As follows from this figure, for all values of N_{int} the dependence of $\tilde{q}_k$ on $\tilde{T}_{Rd}$ is well described by a linear function, in agreement with the case reported in [9]. For any given $\tilde{T}_{Rd}$ the values of $\tilde{q}_k$ decrease with increasing N_{int}. The rate of this decrease, however, becomes small for $N_{int} > 10$ and negligible for $N_{int} > 20$. This allows us to restrict our analysis to the case of $N_{int} = 20$, in agreement with the conclusion reached in [16].

The plots of $\tilde{q}_k$ versus $\tilde{\rho}_{Rd} \equiv \rho_{Rd}/\rho_s$ for $\tilde{T}_{Rd} = 1.1$ and 1.2 and $N_{int} = 20$ are shown in Fig. 4. As one can see in this figure, the plots for these values of $\tilde{T}_{Rd}$ are the lines almost parallel to the $\tilde{\rho}_{Rd}$ axis. This allows us to ignore the dependence of $\tilde{q}_k$ on $\tilde{\rho}_{Rd}$ in agreement with the similar result obtained in [9] for $N_{int} = 0$.

The plots of $\tilde{q}_k$ versus $\tilde{T}_{Rd}$ for $\tilde{\rho}_{Rd} = 1$, $N_{int} = 0$ and 20, and $\tilde{q}_h = q_h/(p_0\sqrt{R_v T_0})$ versus $\tilde{T}_{Rd}$ (horizontal line) are shown in Fig. 5. The following values of parameters were used: $T_g = 1000$ K, $T_{Rd} = 600$ K, $R_d = 5$ μm. The intersections between the horizontal and inclined lines give the required values of $\tilde{T}_{Rd}$. For the case of only elastic collisions ($N_{int} = 0$), $\tilde{T}_{Rd} = 1.014$, for the case when the contribution of inelastic collisions with $N_{int} = 20$ is taken into account $\tilde{T}_{Rd} = 1.026$. This result indicates that the contribution of internal degrees of freedom leads to an increase in $\tilde{T}_{Rd}$.

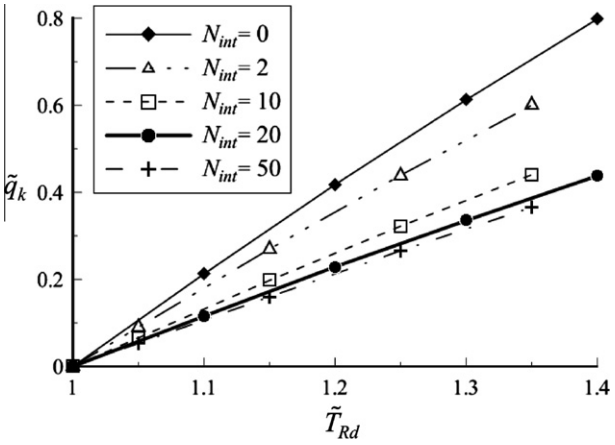

Fig. 3. Plots of normalised heat flux in the kinetic region $\tilde{q}_k \equiv q_k/(p_0\sqrt{R_v T_0})$ versus normalised temperature $\tilde{T}_{Rd} = T_{Rd}/T_s$ for various numbers of internal degrees of freedom N_{int}, assuming that $T_s = T_0 = 600$ K. ρ_{Rd} is taken equal to 0.9 ρ_s.

The plots of $\tilde{j}_k$ versus $\tilde{\rho}_{Rd}$ for $\tilde{T}_{Rd} = 1.026$, $N_{int} = 0$ and 20, and $\tilde{j}_h = j_h/(p_0\sqrt{R_v T_0})$ versus $\tilde{\rho}_{Rd}$ (horizontal line) are shown in Fig. 6. This figure is presented for the same parameters as Fig. 5. Following [9], it was assumed that ρ_{Rd} in Eq. (19) can be replaced with ρ_s.

The intersections between the horizontal and inclined lines give the required values of $\tilde{\rho}_{Rd}$. For the case of only elastic collisions ($N_{int} = 0$), $\tilde{\rho}_{Rd} = 0.968$; for the case when the contribution of inelastic collisions with $N_{int} = 20$ is taken into account, $\tilde{\rho}_{Rd} = 0.926$. This result indicates that the contribution of internal degrees of freedom leads to a decrease in $\tilde{\rho}_{Rd}$.

Similar values of $\tilde{T}_{Rd}$ and $\tilde{\rho}_{Rd}$ were obtained for other values of T_g and R_d relevant for Diesel engine conditions ($T_g = 750$ K and $R_d = 20$ μm) and for values of T_s in the range 300 K to close to the critical temperature. The corresponding values of $\tilde{T}_{Rd}$ and $\tilde{\rho}_{Rd}$ were used for the analysis of heating and evaporation of n-dodecane droplets in realistic Diesel engine-like conditions. The results will be presented in Section 5.

For realistic $\beta < 1$ the values of $\tilde{q}_k$ were practically indistinguishable from those predicted by the model for $\beta = 1$. The plots of $\tilde{j}_k$ versus $\tilde{\rho}_{Rd}$ for $\tilde{T}_{Rd} = 1.026$, $N_{int} = 20$ and $\beta = 1$ and 0.36 are shown in

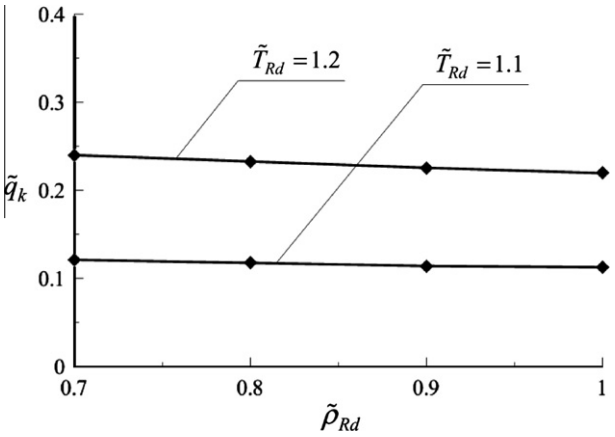

Fig. 4. Plots of normalised heat flux in the kinetic region $\tilde{q}_k$ versus normalised density $\tilde{\rho}_{Rd} = \rho_{Rd}/\rho_s$ for $N_{int} = 20$ and $\tilde{T}_{Rd} = 1.1$ and 1.2.

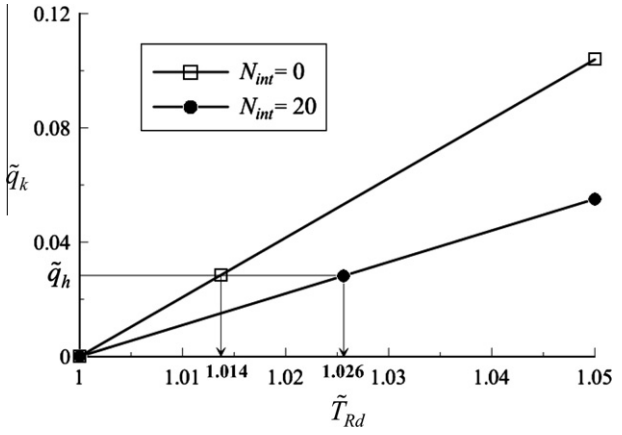

Fig. 5. Plots of $\tilde{q}_k$ versus $\tilde{T}_{Rd}$ for $N_{int} = 0$ and 20, and the plot of $\tilde{q}_h \equiv q_h/(p_0\sqrt{R_v T_0})$ versus $\tilde{T}_{Rd}$ for $T_0 = T_s = 600$ K, $T_g = 1000$ K, $R_{d0} = 5$ μm and $\tilde{\rho}_{Rd} = 1$. The intersections between the plots of $\tilde{q}_k$ and $\tilde{q}_h$ give the required values of $\tilde{T}_{Rd}$.

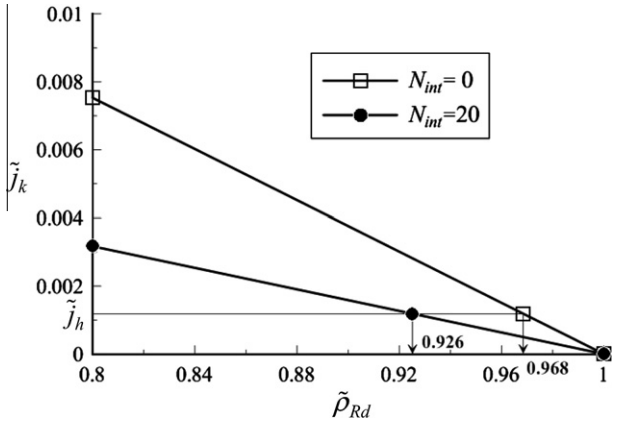

Fig. 6. Plots of $\tilde{j}_k \equiv j_k/(\rho_0\sqrt{R_v T_0})$ versus $\tilde{\rho}_{Rd}$ for $N_{int} = 0$ and 20, and the plot of $\tilde{j}_h \equiv j_h/(\rho_0\sqrt{R_v T_0})$ versus $\tilde{\rho}_{Rd}$ for $T_0 = T_s = 600$ K, $T_g = 1000$ K, $R_{d0} = 5$ μm and $\tilde{T}_{Rd} = 1.026$. The intersections between the plots of $\tilde{j}_k$ and $\tilde{j}_h$ give the required values of $\tilde{\rho}_{Rd}$.

Fig. 7. The plot for $\beta = 1$ is identical to the one shown in Fig. 6, but presented in a wider range of $\tilde{\rho}_{Rd}$. The value of $\beta = 0.36$ is close to the one predicted for $T_s = 600$ K. This will be discussed in Section 6. Note that it would be difficult for us to quantify the error of this estimate of β, due both to the uncertainty of molecular dynamic simulations (only 720 molecules were used) and to extrapolation of the results of these simulations (see Eq. (36).

As follows from Fig. 7, the linear dependence of $\tilde{j}_k$ on $\tilde{\rho}_{Rd}$ is maintained for $\beta = 0.36$, but the values of $\tilde{j}_k$ predicted by the model with $\beta = 0.36$ are lower than those predicted by the model with $\beta = 1$. The values of the mass flux for other values of $\beta > 0.36$ are expected to lie between the plots corresponding to $\beta = 0.36$ and $\beta = 1$. We follow the same procedure of calculating $\tilde{\rho}_{Rd}$ as described earlier for $\beta = 1$ and shown in Fig. 6. As one can see from Fig. 7, this leads to the prediction of lower values of $\tilde{\rho}_{Rd}$ for $\beta = 0.36$ than for $\beta = 1$. Thus the reduction of β is expected to lead to the enhancement of the kinetic effects.

5. Results ($\beta = 1$)

The algorithm described above was applied to computation of the heating and evaporation of Diesel fuel droplets in a hot gas at two temperatures (750 K and 1000 K). The initial droplet temperature and gas pressure in all cases were assumed equal to 300 K and 30 bar respectively. The initial droplet radii were assumed to be equal to 5 μm. Droplets were assumed to be

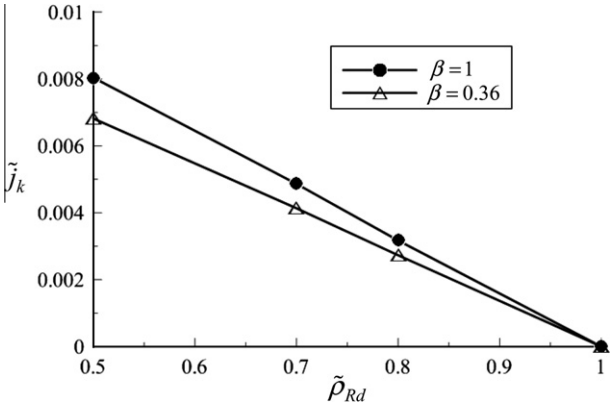

Fig. 7. Plots of $\tilde{j}_k$ versus $\tilde{\rho}_{Rd}$ for $N_{int} = 20$ and $\beta = 1$ and 0.36 versus $\tilde{\rho}_{Rd}$ for $T_0 = T_s = 600$ K, $T_g = 1000$ K, $R_{d0} = 5$ μm and $\tilde{T}_{Rd} = 1.026$.

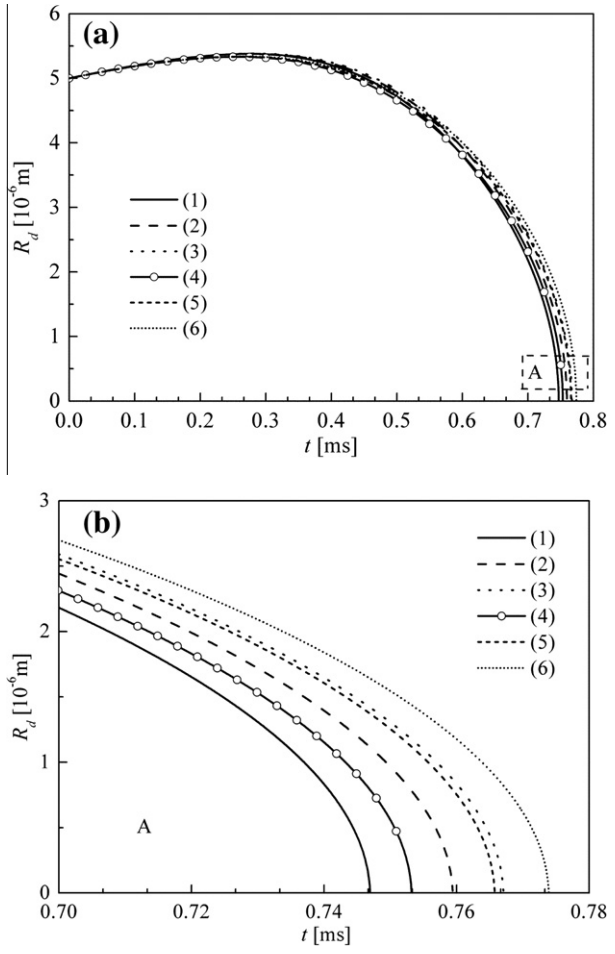

Fig. 8. Plots of R_d versus time t for an n-dodecane droplet, predicted by the hydrodynamic ITC model (Curves 1), the kinetic ITC model, ignoring the effects of inelastic collisions (Curves 2), the kinetic ITC model, taking into account the effects of inelastic collisions (Curves 3), the hydrodynamic ETC model (Curves 4), the kinetic ETC model, ignoring the effects of inelastic collisions (Curves 5), and the kinetic ETC model, taking into account the effects of inelastic collisions (Curves 6) (a). Zoomed part of (a) showing the plots at the final stage of the evaporation process (b). All plots are shown for $T_g = 750$ K, $T_{d0} = 300$ K, $R_{d0} = 5$ μm.

stationary, but the effect of swelling was taken into account. The calculations were performed using the Infinite Thermal Conductivity (ITC) and Effective Thermal Conductivity (ETC) models for the liquid phase, conventional hydrodynamic model, described in Section 2, and kinetic models taking and not taking into account the effects of inelastic collisions. The value of the evaporation coefficient was assumed equal to 1 in all cases.

The results of calculation of the radii and surface temperatures of droplets immersed into gas with temperature 750 K are shown in Figs. 8 and 9, respectively. As follows from Fig. 9, at the initial stage of droplet heating and evaporation, the kinetic effects on temperature are negligible, but the difference in temperatures, predicted by the hydrodynamic models taking and not taking into account the effects of liquid finite thermal conductivity, is quite noticeable. This is consistent with the results earlier reported in [58]. Initially the droplet surface temperature, predicted by the ETC model is larger than the one predicted by the ITC model, as expected. This larger droplet surface temperature predicted by the ETC model leads to the reduction of the heat flux supplied to the droplet, which eventually leads to the situation when the droplet surface temperature predicted by the ETC model becomes smaller than the one predicted by the ITC model. This happens at times close to 0.4 ms. Smaller temperatures, predicted by the ETC model at this stage, lead to slightly slower evaporation rate and longer evaporation time of droplets as shown in Fig. 8.

As follows from Fig. 8, the kinetic models, taking and not taking into account inelastic collisions, predict longer evaporation times compared with the hydrodynamic ETC and ITC models, in agreement with the prediction of the model described in [9]. The kinetic model, taking into account inelastic collisions, predicts longer evaporation times compared with the model ignoring this effect, in agreement with the prediction of Fig. 6. Similar enhancement of the kinetic effects due to the contribution of inelastic collisions can be observed from the temperature curves shown in Fig. 9.

The results of calculation of the radii and surface temperatures of droplets immersed into gas with temperature 1000 K are shown in Figs. 10 and 11, respectively. As in the case shown in Fig. 9, it follows from Fig. 11 that at the initial stage of droplet heating and evaporation, the kinetic effects on temperature are negligible, but the difference in temperatures, predicted by the hydrodynamic models taking and not taking into account the effects of liquid finite thermal conductivity, is noticeable. Initially the droplet surface temperature predicted by the ETC model is larger than the one predicted by the ITC model as expected, but at times larger than about 0.25 ms the surface temperature predicted by the ETC model becomes smaller than the one predicted by the ITC model. In contrast to the case shown in Fig. 8, in the case shown in Fig. 10 the net effects of the increase of the temperature predicted by the ETC model before 0.25 ms and its decrease at times after 0.25 ms lead to shorter evaporation time predicted by the ETC model compared with the ITC model.

As in the case shown in Figs. 8 and 9, for gas temperature equal to 1000 K the kinetic models, taking and not taking into account inelastic collisions, predict longer evaporation times and higher temperatures at the final stage of droplet evaporation, compared with the hydrodynamic ETC and ITC models. Also, as in the case shown in Figs. 8 and 9, the kinetic model, taking into account inelastic collisions, predicts longer evaporation times and higher

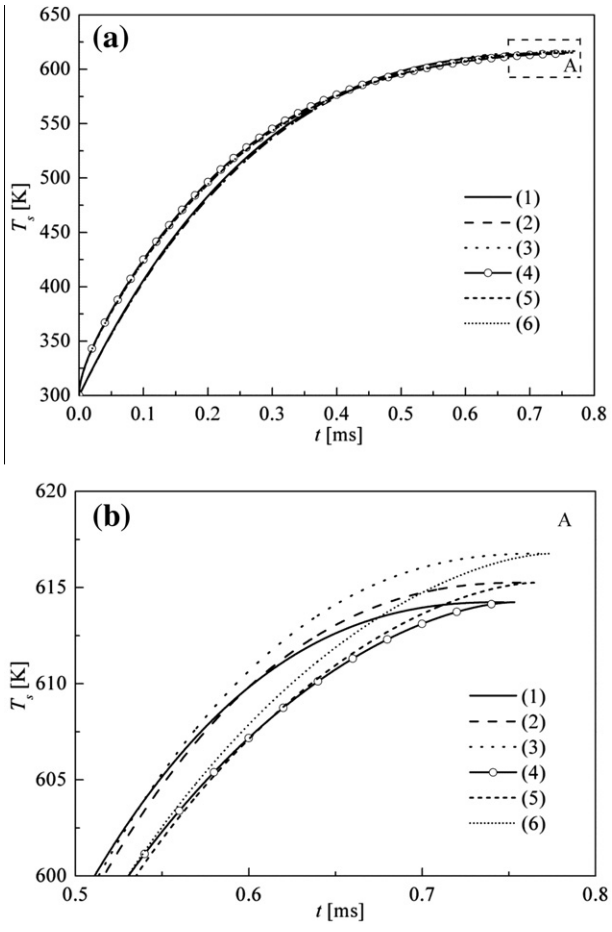

Fig. 9. The same as Fig. 8 but for T_s.

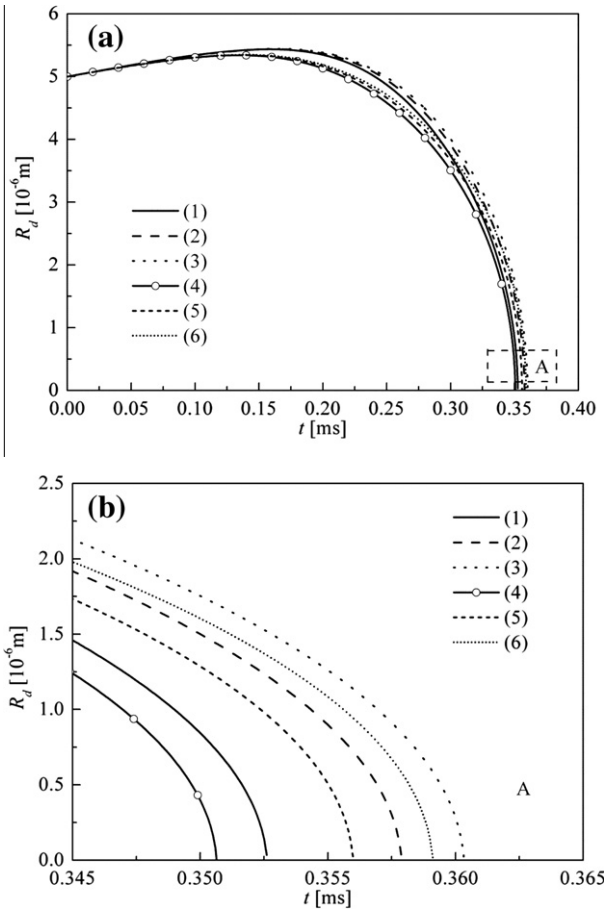

Fig. 10. The same as Fig. 8 but for T_g = 1000 K.

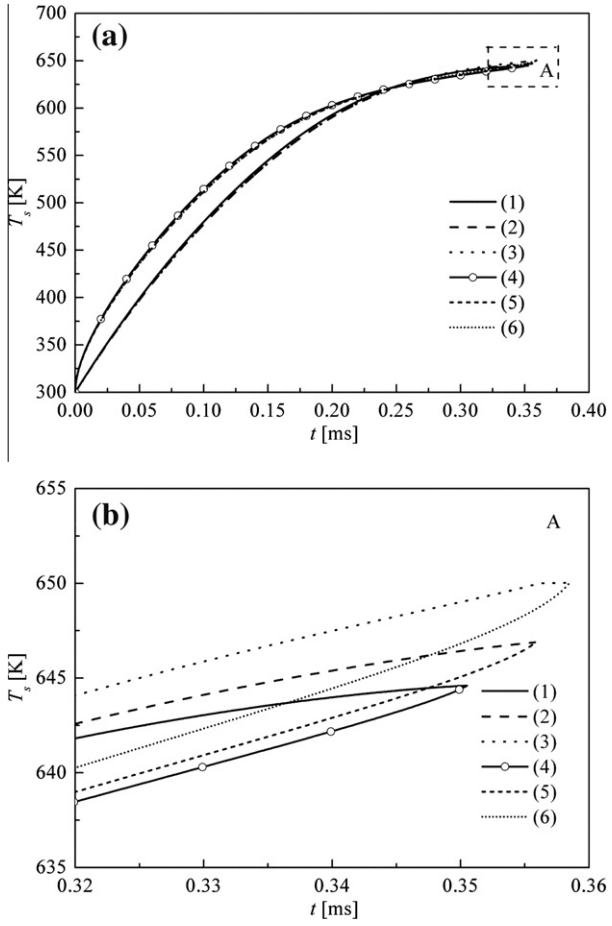

Fig. 11. The same as Fig. 9 but for T_g = 1000 K.

temperatures at the final stage of droplet evaporation, compared with the model ignoring this effect. These kinetic effects are stronger in the case shown in Figs. 10 and 11 than in the case shown in Figs. 8 and 9.

6. Results (β < 1)

As mentioned earlier, in our previously described kinetic models we assumed that β = 1 (see [7–10]). This was justified by the fact that no reliable experimental data or theoretical predictions of β were available at that time. The situation changed after the publication of papers [17,18], where a new model for molecular dynamic simulations of n-dodecane was suggested. Using this model, the authors of [17,18] obtained the values of β at various surface temperatures relevant to Diesel engine conditions. These values are shown in the following table, based on the most comprehensive calculations presented in [18].

The temperature dependence of β inferred from Table 1 can be approximated as:

$$\beta(T_s) = 7 \times 10^{-6} T_s^2 - 9.8 \times 10^{-3} T_s + 3.7215. \quad (36)$$

For T_s = 600 K Eq. (36) predicts β = 0.36. This value of β was used for the plot presented in Fig. 7.

In what follows the effects of β < 1 on n-dodecane droplet heating and evaporation will be presented for the ITC model only. These effects for the ETC model are similar to those for the ITC model.

The results of calculation of the radii and surface temperatures of droplets with initial radii equal to 5 μm immersed into gas with temperature 1000 K using the ITC model with β = 1 and β predicted

Table 1
Condensation/evaporation coefficient as a function of the liquid temperature.

T_s (K)	β
400	0.93
450	0.72
500	0.59
550	0.45

by Eq. (36) are shown in Fig. 12. The plots for β = 1 are the same as shown in Figs. 10 and 11. As one can see from this figure, the effect of β < 1 on droplet radius and temperature in this case is small and can be safely ignored in most practical applications. For gas temperature equal to 750 K this effect is even smaller than in the case of gas temperature equal to 1000 K. This means that the results of the analysis for β = 1 presented in Section 5 and in our previous papers ([7–10]) are applicable for the realistic case β < 1.

Let us now consider a hypothetical case when a droplet with initial radius equal to 5 μm is immersed into gas with temperature 1500 K. The results of calculation of the radii and surface temperatures of droplets in this case are shown in Fig. 13. As one can see from this figure, in this case the effect of β < 1 is much more visible than in the case shown in Fig. 12. This effect leads to increased droplet evaporation time, thus enhancing the kinetic

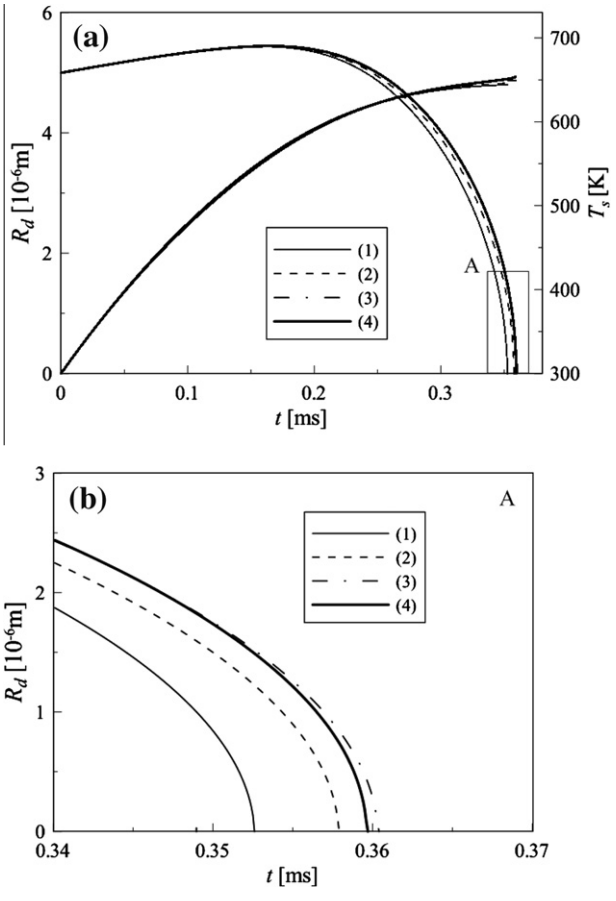

Fig. 12. Plots of R_d and T_s versus time t for an n-dodecane droplet, predicted by the hydrodynamic ITC model (Curves 1), the kinetic ITC model, ignoring the effects of inelastic collisions and non-unity of β (Curves 2), the kinetic ITC model, taking into account the effects of inelastic collisions but ignoring the non-unity of β (Curves 3), and the kinetic ITC model, taking into account the effects of inelastic collisions and the non-unity of β, which is calculated based on Eq. (36) (Curves 4) (a). Zoomed part of (a) showing the values of R_d at the final stage of the evaporation process (b). All plots are shown for T_g = 1000 K, T_{d0} = 300 K, R_{d0} = 5 μm.

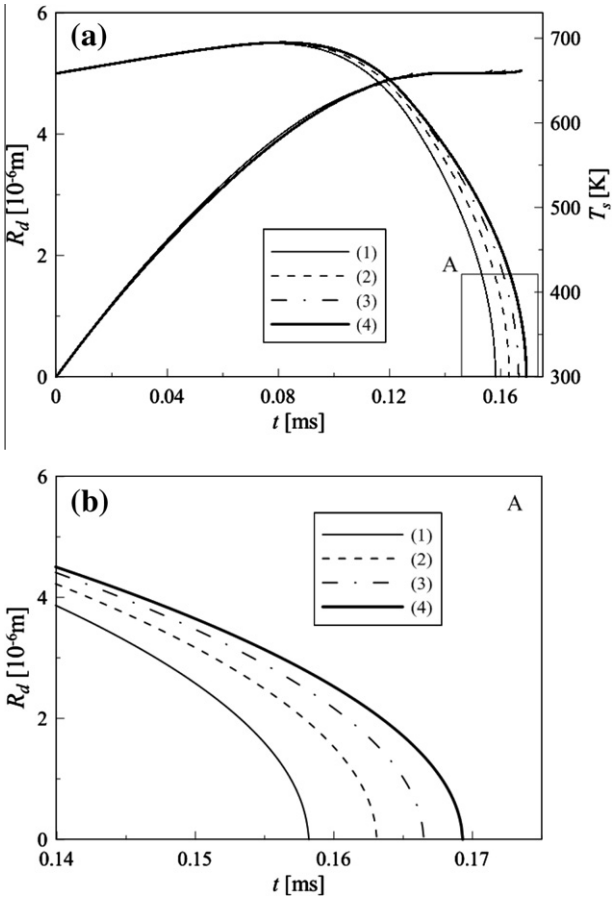

Fig. 13. The same as Fig. 12 but for T_g = 1500 K.

corrections to the prediction of the hydrodynamic model. Note that in the case of this gas temperature, the droplet surface temperature approaches the critical temperature at the final stage of droplet evaporation. In this case the hydrodynamic model used in our analysis is expected to contain uncontrollable errors.

As to the computational efficiency of the model, we note that for a PC Intel Core (TM) 2 Quad CPU Q9550 2.83 GHz with 3.00 GB RAM (only one processor used) in a 32-bit Operating System, the kinetic calculations required about two hours for one case for a given surface temperature. Hydrodynamic calculations required just a few minutes.

At this stage it would be difficult (although not impossible) to perform the validation of the results shown in Figs. 8–13, as the corrections due to the kinetic effects are comparable with errors of measurements of the input parameters of the model. The latter include gas temperature, droplet temperature and radius, gas velocity and others. These results, however, clearly show the errors which would be expected if the kinetic effects are ignored. It is unlikely that kinetic calculations will ever be incorporated into computational fluid dynamics (CFD) codes. The results of these calculations, however, can potentially be approximated by simple formulae as the perturbations to the hydrodynamic calculations. The preliminary results in this direction were discussed in [10].

7. Conclusions

The previously developed kinetic model for droplet heating and evaporation into a high pressure background gas (air) has been generalised to take into account the combined effects of inelastic collisions in the kinetic region, a non-unity evaporation coefficient and temperature gradient inside droplets. The Infinite Thermal Conductivity (ITC) and Effective Thermal Conductivity (ETC) liquid phase models have been used in the analysis. The effects of inelastic collisions have been investigated based on the model developed in [16]. The values of the evaporation coefficient, used in the analysis, have been obtained in [18] based on the molecular dynamics simulation of n-dodecane molecules. As in [9] both heat and mass transfer in the kinetic region have been taken into account. The boundary conditions at the outer boundary of the kinetic region have been introduced by matching the mass fluxes of vapour leaving the kinetic region and entering into the surrounding hydrodynamic region, and the corresponding heat fluxes.

It has been pointed out that for the parameters typical for Diesel engine-like conditions, the heat flux in the kinetic region is a linear function of the vapour temperature at the outer boundary of this region, but practically does not depend on vapour density at this boundary for all models, including and not including the effects of inelastic collisions, and including and not including the effects of a non-unity evaporation coefficient. For any given temperature at the outer boundary of the kinetic region the values of the heat flux have been shown to decrease with increasing numbers of internal degrees of freedom of the molecules. The rate of this decrease has been shown to be strong for small numbers of these degrees of freedom but becomes negligible when the number of degrees of freedom exceeded 20.

The mass flux at this boundary has been shown to decrease almost linearly with increasing vapour density at the same location for all above-mentioned models, as in the case considered in [9]. For any given vapour density at the outer boundary of the kinetic region, the values of the mass flux have been shown to be smaller for the model taking into account the contribution of internal degrees of freedom than for the model ignoring these degrees of freedom (taking into account the contribution of only elastic collisions). Remembering these properties of the heat and mass fluxes, and using the matching conditions at the outer boundary of the kinetic region, the values of temperature and fuel vapour density at this boundary have been found following the procedure earlier described in [9].

It has been shown that the effects of inelastic collisions lead to a stronger increase in the predicted droplet evaporation time in Diesel engine-like conditions relative to the prediction of the hydrodynamic model, compared with the similar increase predicted by the kinetic model considering only elastic collisions. The effects of a non-unity evaporation coefficient have been shown to be noticeable for gas temperatures of 1500 K. At the initial stage of droplet heating and evaporation the surface temperatures predicted by the ETC model have been shown to be larger that those predicted by the ITC model, in agreement with our earlier results (e.g. [58]).

The application of the rigorous kinetic model, taking into account the effects of inelastic collisions, a non-unity evaporation coefficient, and the ETC model, is recommended when accurate predictions of the values of droplet surface temperature and evaporation time in Diesel engine-like conditions are essential.

Acknowledgements

The authors are grateful to EPSRC (UK) (Project EP/H001603/1) and the Russian Foundation for Basic Research (Grants 12-08-90005 and 10-08-00614) for their financial support of this project.

References

[1] I. Langmuir, The dissociation of hydrogen into atoms. Part 2: Calculation of the degree of dissociation and the heat of formation, J. Am. Chem. Soc. 37 (1915) 417–458.
[2] N.A. Fuchs, Evaporation and Droplet Growth in Gaseous Media, Pergamon Press, London, 1959.

[3] A.M. Briones, J.S. Ervin, S.A. Putnam, L.W. Byrd, J.G. Jones, A novel kinetically-controlled de-pinning model for evaporating water microdroplets, Int. Comm. Heat Mass Transfer 39 (2012) 1311–1319.
[4] S. Pati, S. Chakraborty, S.K. Som, Influence of ambient vapor concentration on droplet evaporation in a perspective of comparison between diffusion controlled model and kinetic model, Int. J. Heat Mass Transfer 54 (2011) 4580–4584.
[5] A.P. Kryukov, V.Yu. Levashov, S.S. Sazhin, Evaporation of Diesel fuel droplets: kinetic versus hydrodynamic models, Int. J. Heat Mass Transfer 47 (2004) 2541–2549.
[6] S.S. Sazhin, Advanced models of fuel droplet heating and evaporation, Prog. Energy Combust. Sci. 32 (2006) 162–214.
[7] I.N. Shishkova, S.S. Sazhin, A numerical algorithm for kinetic modelling of evaporation processes, J. Comput. Phys. 218 (2006) 635–653.
[8] S.S. Sazhin, I.N. Shishkova, A.P. Kryukov, V.Yu. Levashov, M.R. Heikal, Evaporation of droplets into a background gas: kinetic modelling, Int. J. Heat Mass Transfer 50 (2007) 2675–2691.
[9] S.S. Sazhin, I.N. Shishkova, A kinetic algorithm for modelling the droplet evaporation process in the presence of heat flux and background gas, Atom. Sprays 19 (2009) 473–489.
[10] S.S. Sazhin, I.N. Shishkova, M.R. Heikal, Kinetic modelling of fuel droplet heating and evaporation: calculations and approximations, Int. J Eng. Syst. Model. Simulat. 2 (2010) 169–176.
[11] P.F. Flynn, R.P. Durrett, G.L. Hunter, A.O. zur Loye, O.C. Akinyemi, J.E. Dec, C.K. Westbrook, Diesel combustion: an integrated view combining laser diagnostics, chemical kinetics, and empirical validation, SAE report 1999-01-0509; 1999.
[12] G. Stiesch, Modelling Engine Sprays and Combustion Processes, Springer, Berlin, London, UK, 2003.
[13] C. Bertoli, M. na Migliaccio, A finite conductivity model for diesel spray evaporation computations, Int. J. Heat Fluid Flow 20 (1999) 552–561.
[14] C. Maqua, G. Castanet, F. Grisch, F. Lemoine, T. Kristyadi, S.S. Sazhin, Monodisperse droplet heating and evaporation: experimental study and modelling, Int. J. Heat Mass Transfer 51 (2008) 3932–3945.
[15] T. Kristyadi, V. Deprédurand, G. Castanet, L. Lemoine, S.S. Sazhin, A. Elwardany, E.M. Sazhina, M.R. Heikal, Monodisperse monocomponent fuel droplet heating and evaporation, Fuel 89 (2010) 3995–4001.
[16] I.N. Shishkova, S.S. Sazhin, J.-F. Xie, A solution of the Boltzmann equation in the presence of inelastic collisions, J. Comput. Phys. (2012), http://dx.doi.org/10.1016/j.jcp.2012.07.007.
[17] B.-Y. Cao, J. -F Xie, S.S. Sazhin, Molecular dynamics study on evaporation and condensation of n-dodecane at liquid-vapour phase equilibria, J. Chem. Phys. 134 (2011) 164309.
[18] J.-F. Xie, S.S. Sazhin, B.-Y. Cao, Molecular dynamics study of the processes in the vicinity of the n-dodecane vapour/liquid interface, Phys. Fluids 23 (2011) 112104.
[19] J. -F Xie, S.S. Sazhin, B.-Y. Cao, Molecular dynamics study of condensation/evaporation and velocity distribution of n-dodecane at liquid-vapour phase equilibria, J. Therm. Sci. Tech. 7 (2012) 288–300.
[20] S.S. Sazhin, P.A. Krutitskii, I.G. Gusev, M.R. Heikal, Transient heating of an evaporating droplet, Int. J. Heat Mass Transfer 53 (2010) 2826–2836.
[21] S.S. Sazhin, P.A. Krutitskii, I.G. Gusev, M.R. Heikal, Transient heating of an evaporating droplet with presumed time evolution of its radius, Int. J. Heat Mass Transfer 54 (2011) 1278–1288.
[22] S.L. Mitchell, M. Vynnycky, I.G. Gusev, S.S. Sazhin, An accurate numerical solution for the transient heating of an evaporating spherical droplet, Appl. Math. Comput. 217 (2011) 9219–9233.
[23] S.S. Sazhin, I.G. Gusev, P.A. Krutitskii, M.R. Heikal, Transient heating of a semitransparent spherical body immersed into a gas with inhomogeneous temperature distribution, Int. J. Therm. Sci. 50 (2011) 1215–1222.
[24] V.S. Galkin, M.N. Kogan, O.G. Fridlender, Some kinetic effects in continuum flows, Fluid Dyn. 5 (1970) 364–371.
[25] M.N. Kogan, N.K. Makashev, On the role of the Knudsen layer in the theory of heterogeneous reactions and flows with the surface reactions, Reports of the Academy of Sciences of USSR. Mechanics of Liquids and Gases 6 (1971) 3–11 (in Russian).
[26] Y. Sone, K. Aoki, S. Takata, H. Sugimoto, A.V. Bobylev, Inappropriateness of the heat-conduction equation for description of a temperature field of a stationary gas in the continuum limit: examination by asymptotic analysis and numerical computation of the Boltzmann equation, Phys. Fluids 8 (1996) 628–638 (8 (1996), 841(E)).
[27] Y. Sone, S. Takata, H. Sugimoto, On the behaviour of a gas in the continuum limit in the light of kinetic theory: the case of cylindrical Couette flows with evaporation and condensation, Phys. Fluids 8 (1996) 3403–3413 (10 (1998), 1239 (E)).
[28] Y. Sone, Kinetic Theory and Fluid Dynamics, Birkhäuser, Springer, 2002.
[29] S. Takata, K. Aoki, Two-surface problems of a multicomponent mixture of vapors and noncondensable gas, Phys. Fluids 11 (1999) 2743–2756.
[30] E.M. Sazhina, S.S. Sazhin, M.R. Heikal, V.I. Babushok, R. Johns, A detailed modelling of the spray ignition process in diesel engines, Combust. Sci. Technol. 160 (2000) 317–344.
[31] E.M. Kartashov, Analytical Methods in the Thermal Conductivity Theory of Solids, Vyshaya Shkola, Moscow, 2001 (in Russian).
[32] H.S. Carslaw, J.C. Jaeger, Conduction of Heat in Solids, Clarendon Press, Oxford, 1986 (Chapter 9).
[33] S.S. Sazhin, P.A. Krutitskii, W.A. Abdelghaffar, S.V. Mikhalovsky, S.T. Meikle, M.R. Heikal, Transient heating of diesel fuel droplets, Int. J. Heat Mass Transfer 47 (2004) 3327–3340.
[34] B. Abramzon, W.A. Sirignano, Droplet vaporization model for spray combustion calculations, Int. J. Heat Mass Transfer 32 (1989) 1605–1618.
[35] S.S. Sazhin, P.A. Krutitskii, A conduction model for transient heating of fuel droplets, in: H.G.W. Begehre, R.P. Gilbert, M.W. Wong (Eds.), Progress in Analysis, Proceedings of the 3rd International ISAAC (International Society for Analysis, Applications and Computations) Congress (August 20–25, 2001, Berlin), vol. II, World Scientific, Singapore, 2003, pp. 1231–1239.
[36] B. Abramzon, S. Sazhin, Convective vaporization of fuel droplets with thermal radiation absorption, Fuel 85 (2006) 32–46.
[37] N.B. Vargaftik, Yu.K. Vinogradov, V.S. Yargin, Handbook of Physical Properties of Liquid and Gases, Begell House, New York, 1996.
[38] G.F. Hewitt (Ed.), Heat Exchanger Design Handbook, vol. 4, Begell House, New York, 2002.
[39] R.B. Bird, W.E. Stewart, E.N. Lightfoot, Transport Phenomena, John Wiley & Sons, 2002.
[40] A.E. Elwardany, I.G. Gusev, G. Castanet, F. Lemoine, S.S. Sazhin, Mono- and multi-component droplet cooling/heating and evaporation: comparative analysis of numerical models, Atom. Sprays 21 (2011) 907–931.
[41] P. Atkins, J. de Paula, Atkins' Physical Chemistry, Seventh ed., Oxford University Press, 2002.
[42] A. Santos, A simple model kinetic equation for inelastic Maxwell particles, in: M.S. Ivanov, A.K. Rebrov (Eds.), Proceedings of the 25th International Symposium on Rarefied Gas Dynamics, July 21–28th 2006, St Petersburg, Russia, Publishing House of the Siberian Branch of the Russian Academy of Sciences, Novosibirsk, 2006, pp. 191–196. ISBN 978.
[43] C. Borgnakke, P.S. Larsen, Statistical collision model for Monte Carlo simulation of polyatomic gas mixture, J. Comput. Phys. 18 (1975) 405–420.
[44] I.S. Tilinin, Impact-parameter dependence of inelastic energy losses in slow atom-atom collisions, Nucl. Instrum. Methods Phys. Res. B 115 (1996) 102–105.
[45] K. Koura, Improved null-collision technique in the direct simulation Monte Carlo method: application to vibrational relaxation of nitrogen, Comput. Math. Appl. 35 (1998) 139–154.
[46] L. Ferrari, A. Carbognani, Differential kinetic equations for a Rayleigh gas with inelastic collisions, Physica A 251 (1998) 452–468.
[47] D. Benedetto, E. Caglioti, The collapse phenomenon in one-dimensional inelastic point particle systems, Physica D 132 (1999) 457–475.
[48] T. Biben, Ph.A. Martin, J. Piasecki, Stationary state of thermostated inelastic hard spheres, Physica A 310 (2002) 308–324.
[49] J. Banasiak, M. Groppi, Solvability of linear kinetic equations with multi-energetic inelastic scattering, Rep. Math. Phys. 52 (2003) 235–253.
[50] N. Fournier, S. Mischler, A spatially homogeneous Boltzmann equation for elastic, inelastic and coalescing collisions, J. Math. Pures Appl. 84 (2005) 1173–1234.
[51] A. Sizhuk, S. Yezhov, The dynamic theory for the inelastically colliding particles, J. Mol. Liquids 127 (2006) 84–86.
[52] R. Lambiotte, M. Ausloos, L. Brenig, J.M. Salazar, Energy and number of collision fluctuations in inelastic gases, Physica A 375 (2007) 227–232.
[53] G.M. Kremer, A.W. Silva, G.M. Alves, On inelastic reactive collisions in kinetic theory of chemically reacting gas mixtures, Physica A 389 (2010) 2708–2718.
[54] G. Furioli, A. Pulvirenti, E. Terraneo, G. Toscani, Convergence to self-similarity for the Boltzmann equation for strongly inelastic Maxwell molecules, Ann. I. H. Poincaré AN 27 (2010) 719–737.
[55] V.V. Aristov, F.G. Tcheremissine, Direct Numerical Solution of the Boltzmann Equation, Computer Centre of the Russian Academy of Sciences, 1992.
[56] A.P. Kryukov, V.Yu. Levashov, I.N. Shishkova, A.K. Yastrebov, The Numerical Solution of the Boltzmann Equation for Engineering Applications, Moscow Power Engineering Institute Publishing House, Moscow, 2005 (in Russian).
[57] N.M. Korobov, Trigonometric Sums and Their Applications, Nauka Publishing House, Moscow, 1989 (in Russian).
[58] S.S. Sazhin, T. Kristyadi, W.A. Abdelghaffar, M.R. Heikal, Models for fuel droplet heating and evaporation: comparative analysis, Fuel 85 (2006) 1613–1630.